IEEE Photonics Journal
An IEEE Photonics Society Publication

Multiplexed Antibody Detection With an Array of Silicon-on-Insulator Microring Resonators

Volume 1, Number 4, October 2009

Katrien De Vos, Student Member, IEEE
Jordi Girones
Tom Claes, Student Member, IEEE
Yannick De Koninck
Stepan Popelka
Etienne Schacht
Roel Baets, Fellow, IEEE
Peter Bienstman, Member, IEEE

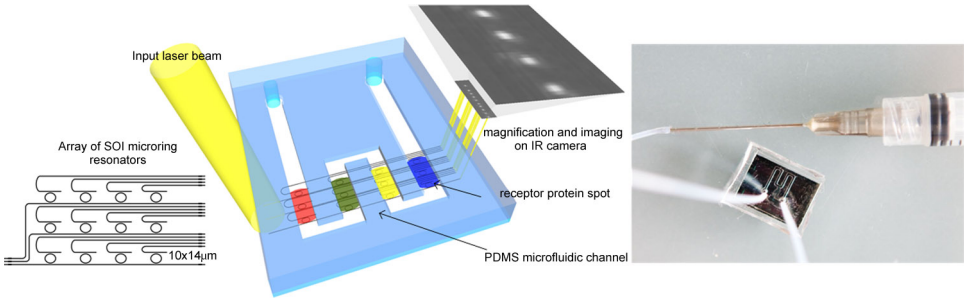

DOI: 10.1109/JPHOT.2009.2035433
1943-0655/$26.00 ©2009 IEEE

Multiplexed Antibody Detection With an Array of Silicon-on-Insulator Microring Resonators

Katrien De Vos,[1] ***Student Member, IEEE*****, Jordi Girones,**[2] **Tom Claes,**[1] ***Student Member, IEEE*****, Yannick De Koninck,**[1] **Stepan Popelka,**[2] **Etienne Schacht,**[2] **Roel Baets,**[1] ***Fellow, IEEE*****, and Peter Bienstman,**[1] ***Member, IEEE***

[1]Photonics Research Group, Department of Information Technology, Ghent University—IMEC, Ghent University, 9000 Gent Belgium
[2]Polymer Chemistry and Biomaterials Research Group, Department of Organic Chemistry, Ghent University, 9000 Gent Belgium

DOI: 10.1109/JPHOT.2009.2035433
1943-0655/$26.00 ©2009 IEEE

Manuscript received September 22, 2009; revised October 18, 2009. First published Online October 22, 2009. Current version published November 13, 2009. This work supported in part by Ghent University under the GOA Project B/05958/01 and in part by IAP 6-10 Photonics@BE. The work of K. De Vos and T. Claes was supported by the Flemish Institute for the Promotion of Innovation through Science and Technology (IWT) under a specialization grant. Corresponding author: K. De Vos (e-mail: Katrien.Devos@intec.ugent.be).

Abstract: Optical cavities are considered promising devices for biosensing to satisfy the high demands of the growing proteomics market. We present a prototype sensor for multiplexed label-free monitoring of biomolecular interactions based on an array of three-by-four silicon-on-insulator microring resonators fabricated by standard complementary metal–oxide semiconductor (CMOS) technology. Parallel readout was performed with an infrared camera. We have demonstrated the simultaneous detection of several model antibodies in a highly specific way. For that, we integrated the optical chip with low-temperature polydimethylsiloxane (PDMS) packaging, enabling excellent compatibility with the receptor molecules. We obtain a very selective biomolecular interaction by grafting a 2.5-nm poly(ethylene glycol) layer to the silicon. Using silicon on insulator as the material platform offers high sensitivity through miniaturization and low-cost mass fabrication through standard CMOS technology steps. The sensors in this interrogation method are able to detect 3.4 pg/mm^2 of a protein overlayer or a theoretical total mass of about 74 ag. For this novel lab on a chip, the fabrication, chemistry, readout, and packaging are developed to be scalable to detect hundreds of affinity interactions within several minutes.

Index Terms: Silicon nanophotonics, biosensors, waveguides, resonators, microfluidics, label-free.

1. Introduction

Label-free monitoring of biomolecular interactions has become of major importance for the emerging proteomics field. While labeled detection methods can be sensitive down to single-molecule detection [1], labels can structurally and functionally alter the assay and the labeling process is labor intensive and costly. Quantification is difficult since the bias label intensity level is dependent on all working conditions [2]. High throughput and high sensitivity are key requirements for label-free biosensors in actual application areas [3]. Biosensors are integrated on an optical chip in various configurations, in order to overcome the limited multiplex possibilities and poor intrinsic

sensitivity of commercially available label-free systems (interferometers [4], [5], gratings [6], [7], plasmonic nanostructures [8] etc.). Optical resonators are considered to be very promising to obtain high sensitivities [9], [10]. Molecular interaction in the near vicinity of an optical cavity changes the refractive index locally, which results in a change of the effective refractive index of the resonant mode, and hence in a resonance wavelength shift. Unlike interferometers, the sensor response does not decrease with decreasing sensor area. The smaller the cavity, the fewer molecules needed to cover the entire surface, while the sensor response does not decrease. This makes optical cavities sensitive to very small amounts of analytes which can be a crucial advantage in some sample-limited applications.

Planar microring resonators are promising implementations of optical cavities for biosensing, because of the mass production possibilities using replica molding or photolithography. Chao *et al.* [11] showed biomolecular detection with planar polymer microring resonators, fabricated by a direct imprinting technique, with a detection limit of 250 pg/mm^2. Xu *et al.* [12] used folded waveguide ring resonators to extend the cavity and increase the Q-factor for higher resolution. They obtain a detection limit of 3 pg/mm^2 or 5-fg total mass. Recently Ramachandran *et al.* [13] applied a planar glass-based microring array in which five microrings were sequentially scanned for rapid molecular detection. In contrast to glasses or polymers, silicon on insulator (SOI) as a material system allows the reuse of standard high-quality CMOS processing facilities, in particular 193-nm lithography. In addition, SOI has a very high refractive index contrast, hence light is highly confined in submicrometer structures and all devices are considerably reduced in size. For example, a single SOI ring resonator used in this study fits on a 10×14 μm^2 area. As a biosensor it benefits from this dimensional advantage twice: as stated before it is sensitive to very small amounts of affinity trapped molecules and allows high-density integration on a single chip. However, targeted deposition of receptor molecules on micrometer-sized sensors is a challenging fluidic problem that might ask for novel concepts. Commercial tools exist to spot proteins down to 5-μm spot size (for example Bioforce Nanospotter), although they have not been widely used so far. The combination of low-cost fabrication and high sensitivity through small dimensions makes SOI a good candidate for disposable biosensor chips.

The quality of a biosensor critically depends on the properties of the chemical surface modification. Protein detection in complex serums requires a highly selective and dense surface functionalization. The interfacial layer has to allow immobilization of receptor molecules and at the same time effectively block non-specific interactions with the macromolecular components of the analyzed sample.

This work demonstrates multiplexed antibody detection with microring resonators integrated on an optical chip. For that we designed an array of three by four SOI ring resonators and developed a measurement system for parallel readout with an infrared camera (see Section 2). The chip is packaged with PDMS microfluidics (Section 3). A monolayer of heterobifunctional poly(ethylene glycol) (PEG) is end-grafted on the SOI chip, providing a stable, reactive and non-fouling coating (see Section 4). Different receptor molecules are covalently linked to different ring resonators by means of spotting (see Section 4). Sensing results are presented in Section 5. In this unique combination of techniques all processes are scalable to high throughput, which makes this platform for disposable chips suitable to be integrated with lab-on-a-chip applications.

2. SOI Microring Array: Chip Design, Readout and Detection Limit

2.1. Chip Layout and Setup

The chip layout and optical setup are illustrated in Fig. 1. Four rings are connected to one common input waveguide, each of them having a dedicated drop signal port. Three of these four-ring series are placed independently next to other. The three input waveguides are simultaneously addressed through vertical grating couplers [14] with a 2-mm-wide collimated beam from a tunable laser source. The output signals of the ring resonators are near-vertically coupled to free space by means of integrated grating couplers and are imaged with an infrared camera. The resonators in series differ by 30 nm in circumference to avoid spectral overlap of resonances. Each resonator has a free spectral range (FSR) of 15 nm and occupies about 150 pm. Up to 20 ring resonators can

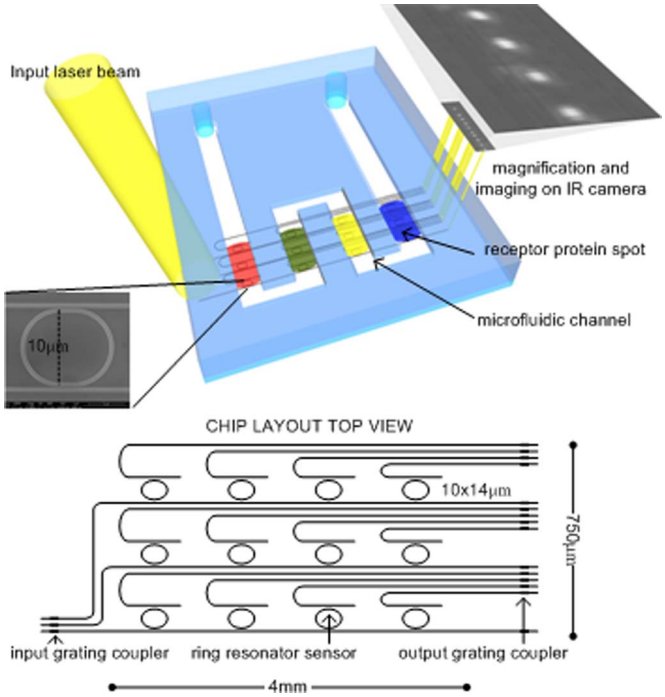

Fig. 1. Illustration of the biosensor platform (not to scale).

be placed in series. The cavities will resonate independently and with similar intensity, and they have about 0.5-nm space to shift during sensing. The drop signals can be collected on one bus waveguide as well, after which the individual signals have to be resolved mathematically from drop- or pass port. This would further decrease the footprint but would not fundamentally alter the results presented here.

The shallow etched gratings are part of the chip design and have maximal coupling efficiency of 31% at 1.55-μm wavelength (40-nm 1-dB bandwidth) for 10° off-vertical coupling angle. Because the bandwidth of the grating couplers is larger than the FSR of the resonators, the grating couplers do not limit the number of resonators placed in series. We do not use space consuming fiber-to-chip coupling. However, the imaging setup is not part of the sensor itself as is usually the case in free-space label-free sensors. This way the optical setup allows for very high alignment tolerances and forms no limitation for high-throughput sensing.

A SANTEC TSL-510 tunable laser was used as a light source. The transmitted light was detected by a XenICs XEVA infrared camera. Input power was chosen so that the intensity of the resonance peaks corresponds to the pixel saturation level to obtain a maximum signal-to-noise ratio. We developed software that captures an image for every wavelength step and stores the maximum intensity values within each dedicated area that overlaps with an output grating coupler spot. Hence, only one number per wavelength and per sensor is stored to avoid memory saturation when scaling the system to large sensor arrays. Postprocessing (fitting of the spectra and tracking of the peaks over time) is automated with MATLAB. The chip was placed on a temperature-stabilized chuck, to avoid drift of the signal, although the signal of a reference sensor can be used to compensate for environmental drift as well. The sample liquids were pumped with a Harvard syringe pump at 5-μl/min flow rate.

The SOI wafers are processed using 193-nm-deep UV lithography and dry etching. The high refractive index contrast enables design of compact and high-density circuits. However, this sets high demands for the fabrication technology, since the spectral characteristics of nano- and microdevices are extremely sensitive to dimensional variations down to a few nanometers. Advanced CMOS

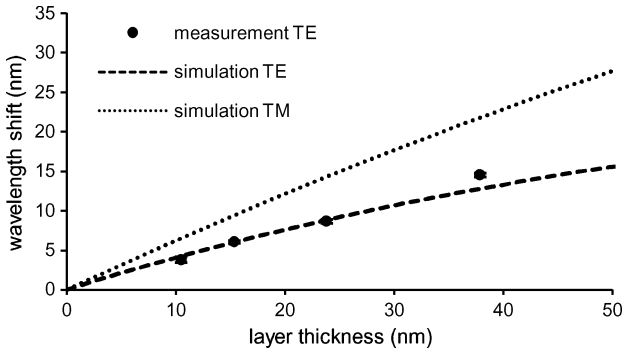

Fig. 2. Comparison between theoretical and experimental response of the resonance wavelength shift to the thickness of SiO_2 overlayer.

fabrication processes are adapted for fabrication of photonics circuits to obtain such high resolution and extreme stability [15].

2.2. Detection Limit

The minimal detectable environmental refractive index change or the detection limit, is determined as the ratio of the minimal resolvable wavelength shift $\Delta\lambda_{min}$ and the sensitivity, the wavelength shift per environmental refractive index change [16]. The refractive index change of the environment can be due to a bulk refractive index change, or an index change near the sensor surface due to biomolecular interaction. The numerator and the denominator of the detection limit definition are discussed, with reflection on our system, in the following paragraphs.

To estimate the sensitivity for interaction near the sensor surface, a simple model of a layer surrounding the waveguides at three sides with constant refractive index and increasing thickness is commonly used [17]. The resonance wavelength shift is

$$\Delta\lambda = \frac{\Delta n_{\text{eff}}\lambda_0}{n_g} \tag{1}$$

taking first-order dispersion into account. Δn_{eff} is the effective index change of the resonating mode, λ_0 the initial resonance wavelength and n_g the group index. We simulate the effective index change Δn_{eff}, using vectorial mode solver software Fimmwave, and calculate the corresponding resonance wavelength shift with formula (1). To verify formula and simulations, we deposited thin layers of SiO_2 on ring resonator sensors and measured the wavelength shift. Fig. 2 shows good correspondence between simulations and experiment. The simulation parameters, thickness and refractive index of the deposited layers, were determined with a M-2000FI Spectroscopic Ellipsometer (J.A. Woollam) on flat simultaneously treated surfaces. Sidewall layer thickness was determined by focused ion beam (FIB) cross-sectional examination of the waveguides. Four rings with different radii were measured for each data point. Average and standard deviation, although very small, are indicated. As expected, the shift does not vary with the ring radius. Sensing with TM polarized light is 1.5 times more sensitive for thin layers, but the grating coupler design for these experiments was optimized for TE polarization.

The detection resolution, the minimal resolvable wavelength shift $\Delta\lambda_{min}$, depends on the shape of the resonance spectrum and on the detection method. As for the shape, Hu *et al.* [18] showed the resolution to be primarily dependent on the Q-factor and, to a lesser degree, to the extinction, as long as it exceeds 15 dB. The resonance spectrum of the racetrack resonators is shown in Fig. 3 (design parameters: radius 5 μm, coupling straight sections 2 μm, waveguide dimensions 450 $\times$ 220 nm and coupling gap widths 160 nm). Q-factor and extinction are determined after fitting to a Lorentzian: full width at half maximum $=$ 74 pm, Q-factor $=$ 20 877, and drop extinction $=$ 16 dB.

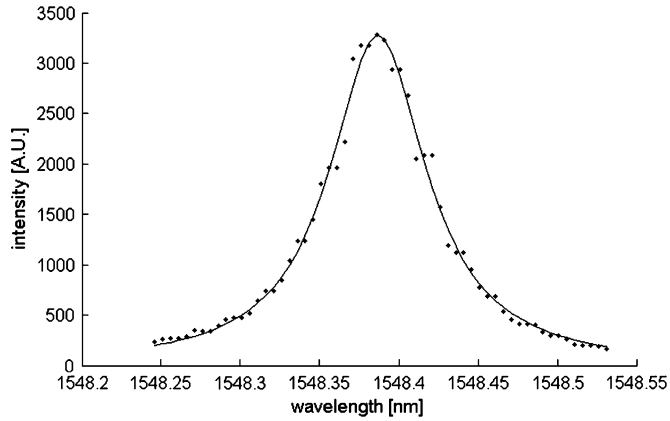

Fig. 3. Spectrum on a drop port of a racetrack resonator, measured with IR camera. Wavelength step: 5 pm. Full width at half maximum: 74 pm, Q-factor = 20 877. Extinction: 16 dB.

The detection method influences $\Delta\lambda_{\text{min}}$ through noise and measurement resolution. Our detection system: wavelength interrogation detection with an infrared camera, is dominated by intensity noise: quantization noise, light source intensity fluctuations and mechanical variations in the coupling (although partly cancelled out by tracking the pixel with maximum intensity). Spectral noise due to temperature fluctuations is suppressed by placing the entire chip and fluidics on a temperature stabilized chuck. Our chosen wavelength step of 5 pm is a compromise between high accuracy and reasonable scan speed (one measurement of the entire array per minute).

In order to calculate $\Delta\lambda_{\text{min}}$ we use a method similar to the method described by Hu *et al.* [18] and by Claes *et al.* [19]. Starting from an analytical spectrum with the measured parameters of Fig. 3, we perform a Monte Carlo analysis by adding 1000 different instantiation of Gaussian noise to the spectrum and fitting the resonance. $\Delta\lambda_{\text{min}}$ is then calculated as

$$\Delta\lambda_{\text{min}} = \sqrt{\frac{\sum(\lambda_{\text{fitted resonance}} - \lambda_{\text{theoretical resonance}})^2}{N}},\ N \text{ the number of iterations.}$$

A different approach that only requires measured data to determine $\Delta\lambda_{\text{min}}$, is to start from the assumption that the actual resonance wavelength is normally distributed with its mean equal to the fitted wavelength and its standard deviation equal to half of the 68.28% confidence interval of the fitted wavelength. Half of the 68.28% confidence interval can than serve as a measure for the minimal resolvable wavelength shift. For the sake of comparison we determined $\Delta\lambda_{\text{min}}$ with both methods and found the results to be in good agreement (see Fig. 4).

To determine the noise of the detection system, the output intensity was measured a large number of times at constant wavelength and constant input power. This was done for a set of input powers to obtain the noise for the full dynamic range of the camera. The intensity noise was then determined as the standard deviation of the normalized power. The same definition was used for the noise in the simulations. Over the dynamic range of the camera, the noise variance ranged from $3 * 10^{-4}$ to $4 * 10^{-4}$. From graph 4 the minimal resolvable wavelength shift for our chip design and detection method is determined to be 0.4 pm.

For this $\Delta\lambda_{\text{min}}$, a layer with average optical thickness of 2.5 pm can be detected (after simulation of the sensitivity with appropriate indices for the optical model of the biolayers: 1.311 water index and 1.45 biolayer index). If the density is approximated as 1.33 g/cm^3 [17], this indicates a molecular layer of approximately 74 ag can be detected, or 3.4-pg/mm^2 mass loading. This corresponds to about 670 molecules of 66-kDa molecular weight.

Previously we reported 10-ng/ml avidin concentration detection limit with SOI microring resonators [20]. With the same receptor molecule coating, with optimized ring resonator design, camera

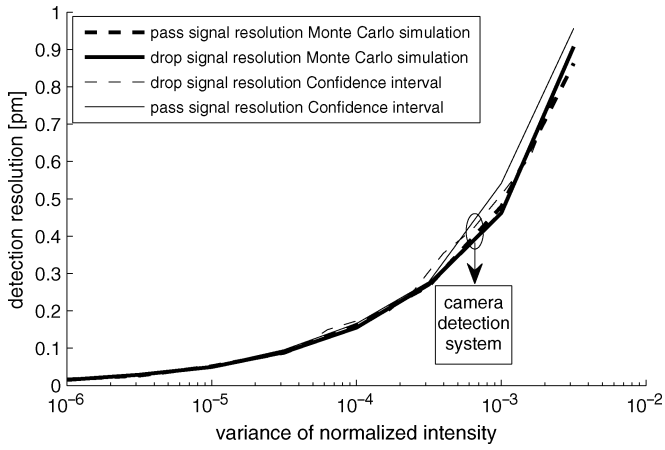

Fig. 4. Minimal detectable wavelength shift $\Delta\lambda_{min}$ versus equipment noise (defined as the variance of the normalized intensity).

readout and accuracy model, the concentration detection limit is for this system is 3 ng/ml. However, the concentration detection limit also depends on receptor molecule density and flow conditions and has to be determined experimentally for various molecular binding pairs. Moreover, a shift equal to $\Delta\lambda_{min}$, does not necessarily originate from a molecular interaction. Caution has to be taken to eliminate all other influences on the resonance wavelength and assure the stability of the entire system (see also Section 5).

3. Microfluidics Packaging

Multiplexed and low-noise detection requires controlled sample delivery. With scalability in mind, different receptor molecules are spotted on the chip before the microfluidic channels are mounted. This is in contrast with the approach in which receptor molecules are coupled to the surface after bonding the channels. This requires a more complex channel network with multiple in- and outlets, especially for large sensor arrays. Our approach asks for a low-temperature bonding process during which no adhesive glue can be in contact with the receptor molecules on the SOI chip. A commonly used technique where both substrates are exposed to a short oxygen plasma treatment and bonded at higher temperature for permanent sealing can therefore not be used [21]. We use a stamp-and-stick method to transfer the channels on the SOI chip without damaging the fragile receptor molecules. This principle has first been described by Satyanarayana *et al.* [22], we adapted this technique for our purpose.

200 $\times$ 50 μm^2 microfluidic channels are fabricated in PDMS by soft lithography. A 7-μm-thick SU-8 glue layer is spincoated on a flat silicon substrate. The PDMS is given a short O2-plasma treatment to enhance adhesion to the glue. After that the PDMS microfluidics chip is stamped in the SU-8 glue layer, after which a thin layer of glue surrounds the channels. A too thick glue layer will clog the channels, a layer that is too thin will not be transferred to the PDMS. The PDMS channels are aligned to the SOI sensor array with a flip-chip bonder, both devices are brought into contact and the SU-8 glue is UV-cured for 2.5 min. Fig. 5 shows a picture of the finished disposable biosensor.

4. Surface Preparation

4.1. Materials

Standard chemicals were purchased from Sigma-Aldrich and used as received, except (3-glycidyloxypropyl)-trimethoxysilane (GOPTS) that was distilled before use. α-tertbutyl-oxycarbonylamino-ω-amino poly(ethylene glycol) (tBoc-DAPEG), MW 2950 was purchased from Rapp Polymere.

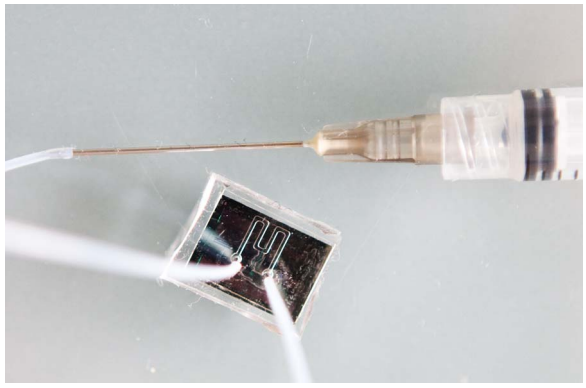

Fig. 5. SOI biosensor chip packaged with PDMS microfluidics.

Human immunoglobulin (Hu-IgG), human serum albumin (HSA), bovine serum albumin (BSA), and specific antibodies for Hu-IgG and HSA (in form of full antiserums developed in goats) were all acquired from Sigma-Aldrich.

Phosphate buffered saline (PBS; pH 7.4, 10-mM phosphate, 150-mM NaCl) was used as a running buffer.

4.2. Preparation of Functional PEG Coating and Immobilization of Proteins

The SOI chips were treated according to a procedure detailed and characterized elsewhere [23]. In brief, SOI chips were cleaned and modified with epoxysilane (GOPTS). Silanized chips were subsequently melt grafted with t-Boc-monoprotected DAPEG. Transducers with t-Boc-protected amino end groups were placed in a vacuum desiccator and stored until needed.

4.3. Immobilization of Proteins on the SOI Surface

Cleavage of t-Boc protecting group from amino groups of PEG was carried out by immersing the chips in trifluoroacetic acid (TFA) for 10 minutes followed by rinsing with MilliQ water and sonication in acetone. For the initial biotin/avidin sensitivity test, direct biotinylation of the amino groups was conducted by immersing the transducers for 2 hr in 2-ml PBS buffer solution to which 100 μl of a solution biotin-LC-NHS (Pierce) in DMF (4mg/ml) was added.

For the protein and biotin-NH_2 experiments (see Section 5), surface amino functions were converted into activated carboxylate groups according to the following procedure [24]: 40 mg of di-succinimidyl carbonate (DSC), 2mg of 4-dimethylamino pyridine (DMAP) and 60 μl of dry triethylamine (TEA) were dissolved in 1 ml of dry DMF. Fifty μl of this solution was deposited on the surface of a sensor and covered with another one. The sandwich was then incubated for 4 hr under dry conditions. After the incubation period, chips were rinsed with methanol and blown dry with argon.

All proteins were spotted at 1-mg/ml concentration in PBS (pH 7.4) containing 10% glycerine to prevent spot evaporation and normalize spot size [25]. Minimal spot size of the BioDot spot tool is 300 μm in diameter, but one column of racetrack resonators occupied about a 1-mm diameter, so that is what we aimed for. Samples were incubated in the fridge at 4 °C overnight. Afterwards, samples were rinsed thoroughly with MilliQ water and PBS. The protein coupling coverage is not fully repeatable yet. The reaction scheme is illustrated in Fig. 6.

5. Biosensing Results

5.1. Preparatory Tests: From Avidin to Antibody Detection

In recent published work we reported a single-microring SOI-based biosensor and demonstrated high response to avidin accumulation on a PEG-coated microring surface with immobilized biotin [19].

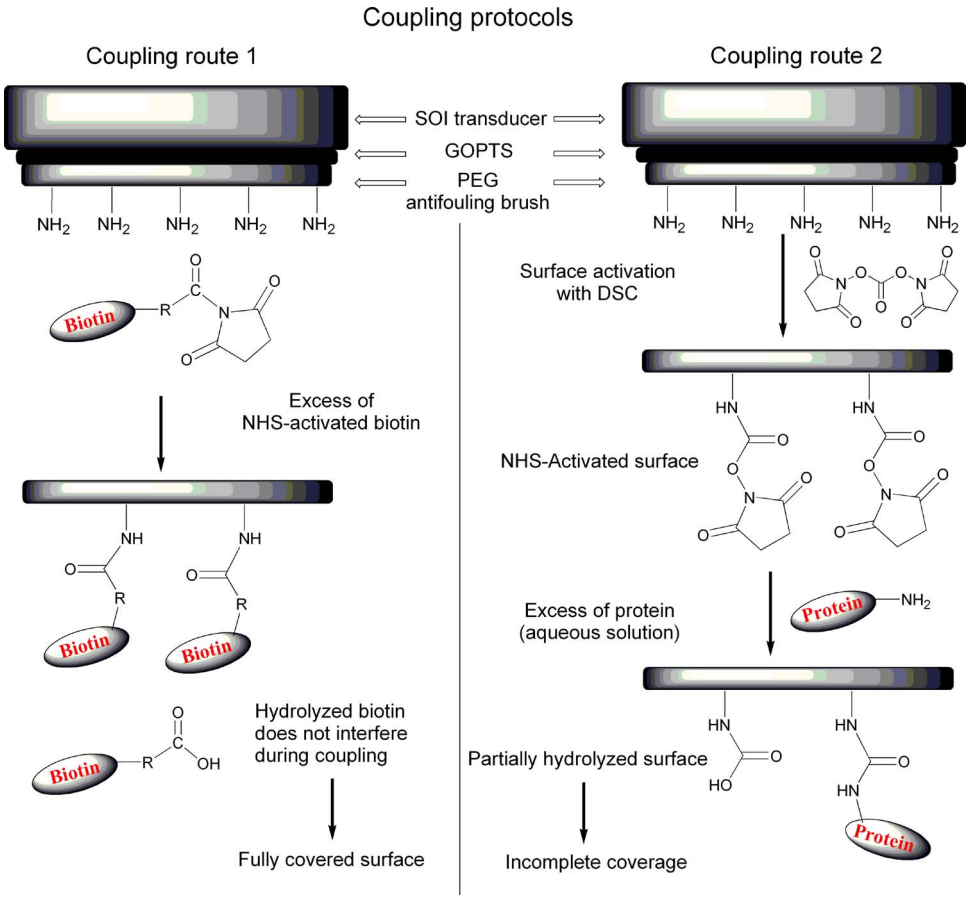

Fig. 6. Employed coupling protocols for immobilization of receptor molecules (biotin and proteins) on SOI microring resonators precoated with a functional PEG layer.

The same high-affinity biotin/avidin pair and PEG coating was applied here (see Fig. 6, coupling route 1) to verify the highly selective signal in complex body fluids (see Fig. 7, full line). After stabilizing the signal in PBS-diluted goat serum (1.9-mg/ml total protein concentration), a sample of the same serum fortified with 1.5 mg/ml of BSA was run through the system showing almost no response. After 1 hr, a sample fortified with 62 μg/ml of avidin was analyzed. Within a few minutes a sharp wavelength shift was detected, which corroborates the high selectivity and sensitivity of the system.

To immobilize protein receptor molecules on the PEG-coated silicon sensor, the original coupling procedure for N-hydroxysuccinimidyl ester of biotin (biotin-NHS) had to be modified since proteins do not bear groups that could react directly with amino groups of the PEG coating. Before the coupling step, the amino end groups of the PEG coating were transformed to N-hydroxysuccinimidyl (see Fig. 6, coupling route 2). The efficiency of the second route was verified and compared to that of the first route using a derivative of biotin with a primary amino group (biotin-NH_2). The avidin binding test revealed that the second route is somewhat less efficient (see Fig. 7, dashed line), probably due to partial hydrolysis of surface NHS-ester groups during the coupling step. Although not optimal yet, this result indicates the viability of the applied methodology.

5.2. Multiplexed Protein Detection

The SOI chips with a PEG coating are modified according to coupling route 2 (see Fig. 6), packaged with microfluidics and placed in the optical setup. Fig. 8 shows the result of a proof-of-principle sensing experiment. Three different proteins are spotted on the resonators: Hu-IgG, HSA

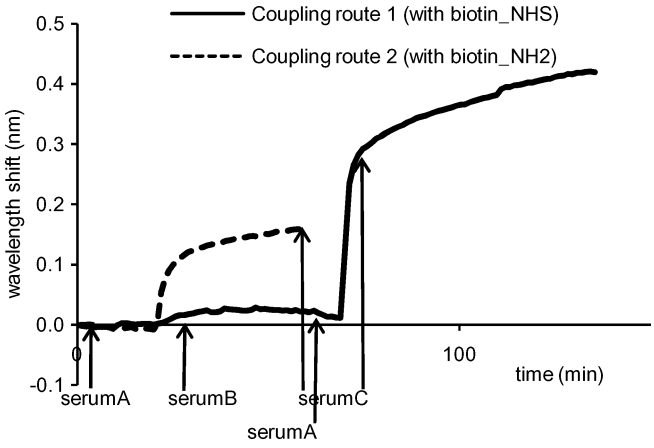

serumA: dilluted goat serum (1.9mg/ml protein concentration)
serumB: 1.5mg/ml BSA in serumA
serumC: 62µg/ml avidin in serumA

Fig. 7. Preparatory test: Biotin-NHS versus biotin-NH_2 as model receptor molecules.

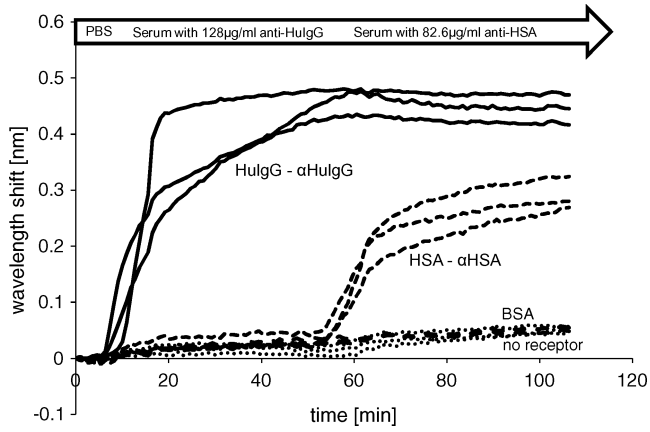

Fig. 8. Experiment with three different recepto molecules spotted on the SOI chip: Hu-IgG, HSA, and BSA. PBS was introduced first to establish the reference. After that, two serums were successively pumped over the sensors. The first serum contained 128 μg/ml anti-Hu-IgG and 1.9 mg/ml other proteins, and the second serum contained 82.6 μg/ml anti-HSA and 1.5 mg/ml other proteins. The resonators spotted with the complementary proteins responded sharply, while the response of the other resonators remained low.

and BSA. The fourth column of resonators was left for reference. First, PBS was pumped over the sensors to set the reference wavelength. After that, two diluted body fluids are successively pumped through the channels; goat serum with 128-μg/ml polyclonal anti-Hu-IgG (1.9-mg/ml total protein concentration) and goat serum with 82.6-μg/ml polyclonal anti-HSA (1.5-mg/ml total protein concentration). All dilutions are made with PBS $+$ 0.1% Tween. Notice the high concentration of non-specific proteins versus the low concentration of the specific antibodies in the serum. When the first serum is introduced, a sharp signal rise was measured for the three resonators covered with Hu-IgG. The other nine resonators barely responded, proving the absence of anti-HSA and anti-BSA in the first serum. Upon introducing the second serum, the signal of the resonators covered with HSA rises sharply, while the other signals remain constant. This indicates the presence of anti-HSA in the second serum and the absence of anti-Hu-IgG and anti-BSA. The non-specific background signal is extremely low. No difference in background signal was detected between the reference sensors and the sensors covered with BSA.

The variation between equally covered sensor signals is mainly due to a slight difference in receptor coverage. Intra-chip variations in waveguide width are very small (< 1 nm) and account for less than 3-pm variation in response between different sensors. Wavelength shifts due to temperature variations are avoided by place the entire chip on a temperature-stabilizing chuck. A small part of the shift is due to the difference in refractive index of the diluted serums versus PBS. This difference is estimated 2.6×10^{-4} for the serum with 1.5-mg/ml protein concentration [17], which corresponds to a shift of 15 pm. The reference signals, both from the BSA sensors and the receptor molecule-free sensors, can be subtracted from the positive signals. This way the non-specific interaction signal and the bulk refractive index signal are eliminated and we obtain the net shift due to specific binding.

6. Conclusion

We demonstrated multiplexed antibody detection in complex samples with an array of three by four SOI microring resonators. All parts of the platform were designed for parallel high-throughput molecular detection. A thin hydrophilic PEG coating serves as intermediate surface layer for two purposes: covalent binding of the receptor proteins and keeping the background signal from non-specific interactions with macromolecular sample components very low. Further optimization of the coupling conditions is likely to increase the receptor density. A stamp-and-stick bonding technique for the aligned microfluidics packaging was used; this offers excellent compatibility with the spotted receptor proteins. Parallel readout of the sensors was obtained by imaging the output signals that are vertically deflected from the chip by means of integrated grating couplers. The software for automated signal capturing and processing is optimized toward low memory usage so that there are no limitations for readout of larger arrays. The entire platform was optimized for high-throughput sample analysis with high sensitivity for disposable lab-on-a-chip devices.

Acknowledgment

The authors thank ePIXfab (www.epixfab.eu) for the fabrication of the SOI devices.

References

[1] W. E. Moerner, "New directions in single-molecule imaging and analysis," *Proc. Nat. Acad. Sci.*, vol. 104, no. 31, pp. 12 596–12 602, Sep. 2007.
[2] X. Yu, D. Xu, and Q. Cheng, "Label-free detection methods for protein microarrays," *Proteomics*, vol. 6, no. 20, pp. 5493–5503, Oct. 2006.
[3] A. J. Qavi, A. L. Washburn, J. Y. Byeon, and R. C. Bailey, "Label-free technologies for quantitative multiparameter biological analysis," *Anal. Bioanal. Chem.*, vol. 394, no. 1, pp. 121–135, May 2009.
[4] A. Ymeti, J. Greve, P. V. Lambeck, T. Wink, S. W. F. M. van Hövell, T. A. M. Beumer, R. Wijn, R. G. Heideman, V. Subramaniam, and J. S. Kanger, "Fast, ultrasensitive virus detection using a young interferometer sensor," *Nano Lett.*, vol. 7, no. 2, pp. 394–397, Feb. 2007.
[5] L. M. Lechuga, K. Zinoviev, L. Fernandez, J. Elizalde, O. E. Hidalgo, and C. Dominguez, "Biosensing microsystem platforms based on the integration of Si Mach-Zehnder interferometer, microfluidics and grating couplers," *Proc. SPIE*, vol. 7220, p. 722 00L, 2009.
[6] X. Wei, C. Kang, G. Rong, S. T. Retterer, and S. M. Weiss, "Porous silicon waveguide with integrated grating coupler for DNA sensing," *Proc. SPIE*, vol. 7167, p. 716 70C, 2009.
[7] S. Grego and B. R. Stoner, "Wavelength interrogation of optical waveguide biosensors in the input grating coupler configuration," *Proc. SPIE*, vol. 7218, p. 721 81A, 2009.
[8] P. P. P. Debackere, S. Scheerlinck, P. Bienstman, and R. Baets, "Surface plasmon interferometer in silicon-on-insulator: Novel concept for an integrated biosensor," *Opt. Express*, vol. 14, no. 16, pp. 7063–7072, Aug. 2006.
[9] F. Vollmer and S. Arnold, "Whispering-gallery-mode biosensing: Label-free detection down to single molecules," *Nat. Methods*, vol. 5, no. 7, pp. 591–596, Jul. 2008.
[10] A. M. Armani, R. K. Kulkarni, S. E. Fraser, R. C. Flagan, and K. J. Vahala, "Label-free, single-molecule detection with optical microcavities," *Science*, vol. 317, no. 5839, pp. 783–787, Aug. 2007.
[11] C. Y. Chao and L. J. Guo, "Polymer microring resonators for biochemical sensing applications," *IEEE J. Sel. Topics Quantum Electron.*, vol. 12, no. 1, pp. 134–142, Jan./Feb. 2006.
[12] D. X. Xu, A. Densmore, A. Delage, P. Waldron, R. McKinnon, S. Janz, J. Lapointe, G. Lopinski, T. Mischki, E. Post, P. Cheben, and J. H. Schmid, "Folded cavity SOI microring sensors for high sensitivity and real time measurement of biomolecular binding," *Opt. Express*, vol. 16, no. 19, pp. 15 137–15 148, Sep. 2008.
[13] A. Ramachandran, S. Wang, J. Clarke, S. J. Ja, D. Goad, L. Wald, E. M. Flood, E. Knobbe, J. V. Hryniewicz, S. T. Chu, D. Gill, W. Chen, O. King, and B. E. Little, "A universal biosensing platform based on optical micro-ring resonators," *Biosens. Bioelectron.*, vol. 23, no. 7, pp. 939–944, Feb. 2008.

[14] W. Bogaerts, R. Baets, P. Dumon, V. Wiaux, S. Beckx, D. Taillaert, B. Luyssaert, J. Van Campenhout, P. Bienstman, and D. Van Thourhout, "Nanophotonic waveguides in silicon-on-insulator fabricated with CMOS technology," *J. Lightw. Technol.*, vol. 23, no. 1, pp. 401–412, Jan. 2005.
[15] S. K. Selvaraja, P. Jaenen, W. Bogaerts, D. Van Thourhout, P. Dumon, and R. G. Baets, "Fabrication of photonic wire and crystal circuits in silicon-on-insulator using 193-nm optical lithography," *J. Lightw. Technol.*, vol. 27, no. 8, pp. 4076–4083, Sep. 2009.
[16] I. M. White and X. Fan, "On the performance quantification of resonant refractive index sensors," *Opt. Express*, vol. 16, no. 2, pp. 1020–1028, Jan. 2008.
[17] J. Vörös, "The density and refractive index of adsorbing protein layers," *Biophys. J.*, vol. 87, no. 1, pp. 553–561, Jul. 2004.
[18] J. Hu, X. Sun, A. Agarwal, and L. C. Kimerling, "Design guidelines for optical resonator biochemical sensors," *J. Opt. Soc. Amer. B, Opt. Phys.*, vol. 26, no. 5, pp. 1032–1041, May 2009.
[19] T. Claes, J. Girones Molera, K. De Vos, E. Schacht, R. Baets, and P. Bienstman, "Label-free biosensing with a slot waveguide based ring resonator in silicon-on-insulator," *IEEE Photon. J.*, vol. 1, no. 3, pp. 197–204, Sep. 2009.
[20] K. De Vos, I. Bartolozzi, E. Schacht, P. Bienstman, and R. Baets, "Silicon-on-insulator microring resonator for sensitive and label-free biosensing," *Opt. Express*, vol. 15, no. 12, pp. 7610–7615, Jun. 2007.
[21] S. Bhattacharya, A. Datta, J. M. Berg, and S. Gangopadhyay, "Studies on surface wettability of poly(dimethyl) siloxane (PDMS) and glass under oxygen-plasma treatment and correlation with bond strength," *J. Microelectromech. Syst.*, vol. 14, no. 3, pp. 590–597, Jun. 2005.
[22] S. Satyanarayana, R. N. Karnik, and A. Majumdar, "Stamp-and-stick room-temperature bonding technique for microdevices," *J. Microelectromech. Syst.*, vol. 14, no. 2, pp. 392–399, Apr. 2005.
[23] K. De Vos, J. Girones, S. Popelka, E. Schacht, R. Baets, and P. Bienstman, "SOI optical microring resonator with poly(ethylene glycol) polymer brush for label-free biosensor applications," *Biosens. Bioelectron.*, vol. 24, no. 8, pp. 2528–2533, Apr. 2009.
[24] A. Wolter, R. Niessner, and M. Seidel, "Preparation and characterization of functional poly(ethylene glycol) surfaces for the use of antibody microarrays," *Anal. Chem.*, vol. 79, no. 12, pp. 4529–4537, Jun. 2007.
[25] E. W. Olle, J. Messamore, M. P. Deogracias, S. D. McClintock, T. D. Anderson, and K. J. Johnson, "Comparison of antibody array substrates and the use of glycerol to normalize spot morphology," *Exp. Mol. Pathol.*, vol. 79, no. 3, pp. 206–209, Dec. 2005.